

A Coupled EXAFS–Molecular Dynamics Study on PuO_2^+ and NpO_2^+ Hydration: The Importance of Electron Correlation in Force-Field Building

Gema Raposo-Hernández, José M. Martínez, Rafael R. Pappalardo, Christophe Den Auwer, and Enrique Sánchez Marcos*



Cite This: *Inorg. Chem.* 2022, 61, 8703–8714



Read Online

ACCESS |



Metrics & More

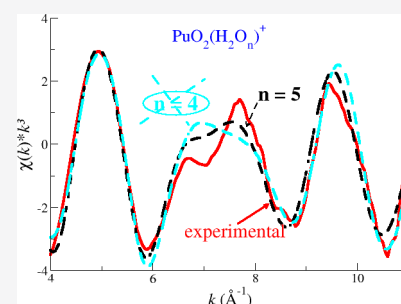


Article Recommendations



Supporting Information

ABSTRACT: The physicochemical properties of the monovalent actinyl cations, PuO_2^+ and NpO_2^+ , in water have been studied by means of classical molecular dynamic simulations. A specific set of cation–water intermolecular potentials based on ab initio potential energy surfaces has been built on the basis of the hydrated ion concept. The TIP4P water model was adopted. Given the paramagnetic character of these actinyls, the cation–water interaction energies were computed from highly correlated wave functions using the NEVPT2 method. It is shown that the multideterminantal character of the wave function has a relevant effect on the main distances of the hydrated molecular cations. Several structural, dynamical, and energetic properties of the aqueous solutions have been obtained and analyzed. Structural RDF analysis gives An– O_{yl} distances of 1.82 and 1.84 Å and An–O(water) distances of 2.51 and 2.53 Å for PuO_2^+ and NpO_2^+ in water, respectively. Experimental EXAFS spectra from dilute aqueous solutions of PuO_2^+ and NpO_2^+ are revisited and analyzed, assuming tetra- and pentahydration of the actinyl cations. Simulated EXAFS spectra have been computed from the snapshots of the MD simulations. Good agreement with the experimental information available is found. The global analysis leads us to conclude that both PuO_2^+ and NpO_2^+ cations in water are stable pentahydrated aqua ions.



INTRODUCTION

The actinyl forms of actinoids are their trans-dioxo molecular cations, $\text{AnO}_2^{+/2+}$, present in the high oxidation states, V and VI.¹ They exhibit high solubilities in water what leads to a rich solution chemistry in a wide set of scenarios where their chemical behavior may be quite different: ligand complexation, hydrolysis processes coupled to acidity or basicity of the medium, adsorption on surfaces, polymerization, and others.^{2–7} It is of primary interest the proper structural characterization of the hydration of such actinyls in order to further understand their physicochemical properties in the different environments that they may face. It has been shown that these actinyls in water are surrounded by water molecules defining stable aqua ions, $[\text{AnO}_2(\text{H}_2\text{O})_n]^{+/2+}$, being generally accepted to have a hydration number of five,^{3,8–13} although four has also been proposed in some cases.^{14–16} The actinyl aqua ion chemistry is intimately joined to nuclear technology due to its role in spent nuclear fuel, reprocessing, temporary and permanent storage, and environmental speciation.^{6,17}

The structural characterization of these cations has been conducted by both experimental and theoretical techniques. Among the experimental ones, the technique giving a more direct information is the X-ray absorption spectroscopy (XAS), in particular the extended X-ray absorption fine structure (EXAFS).^{4,17–20} The great advantage of this technique is its ability to supply short-range structural information around an

specific atom, the absorbing atom, with a structural precision of 0.01 Å for the first coordination shell distance and one unit in the coordination number.^{10,12,19,21,22} Given that no long-range order is needed and submillimolar concentrations of the absorbing atom can be detected, EXAFS is a really powerful and very suitable tool for the study of solutions containing actinoid cations.^{4,17,20,23}

Among the theoretical techniques, quantum-mechanical methods and computer simulations have also provided valuable information. In the first case, the studies usually combine the molecular cation with a small number of water molecules forming the hydrated ion and adding solvent boundary conditions by means of a continuum solvation model.^{24–29} A general solvent molecular description can be reached by using statistical techniques, either assuming ab initio molecular dynamics (AIMD) at reliable QM levels or classical MD simulations employing in this case reliable force fields.

Received: February 10, 2022

Published: May 26, 2022

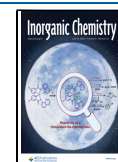


Table 1. Gas-Phase QM and Force-Field Optimizations, MD First-Shell Distances at 300 K, and Debye–Waller factors (σ^2)^a

method	CN	$R_{\text{An-Oyl}}$ (Å)	$\sigma_{\text{An-Oyl}}^2$ (Å ²)	$R_{\text{An-O}_1}$ (Å)	σ^2 (An-O ₁)	ref
[PuO ₂ (H ₂ O) _n] ⁺						
QM(NEVPT2)	5	1.806		2.506		this work
QM(NEVPT2)	4	1.800		2.448		this work
POT5(NEVPT2)	5	1.805		2.505		this work
POT5(NEVPT2)	4	1.799		2.437		this work
POT4(NEVPT2)	4	1.795		2.450		this work
MD_POT5 (300 K)	5	1.822	0.0007	2.507	0.008	this work
MD_POT4 (300 K)	4	1.809	0.00035	2.454	0.0013	this work
EXAFS	4	1.821	0.030	2.48	0.072	Panak et al. ¹⁴
EXAFS	3.3	1.81	0.0020	2.47	0.0044	Di Giandomenico et al. ¹⁵
EXAFS	5.3	1.81	0.002	2.47	0.009	Dalodière et al. ²⁰
QM(B3LYP)	5	1.808		2.61		Hay et al. ²⁵
QM(PBE)	5	1.86		2.53		Rizhkov et al. ³⁵
QM (B3LYP)	5	1.76		2.53		Pomogaev et al. ⁵⁸
MD_POT5 (300 K)	5	1.77		2.56		Pomogaev et al. ⁵⁸
MD/PBE (300 K)	5	1.82		2.55		Oдох et al. ¹⁶
MD/PBE (300 K)	4	1.85		2.47		Oдох et al. ¹⁶
[NpO ₂ (H ₂ O) _n] ⁺						
QM(NEVPT2)	5	1.831		2.522		this work
QM(NEVPT2)	4	1.825		2.466		this work
POT5(NEVPT2)	5	1.825 (1.83)		2.529 (2.52)		this work (Pérez-Conesa et al.) ³⁸
MD_POT5 (300 K)	5	1.842 (1.84)	0.0007 (0.0007)	2.528 (2.54)	0.008 (0.011)	this work (Pérez-Conesa et al.) ³⁸
EXAFS	5	1.822	0.002	2.488	0.006	Reich et al. ⁹
EXAFS	5.2	1.84	0.002	2.49	0.007	Ikeda et al. ¹²
EXAFS	4.4	1.83	0.0056	2.51	0.0040	Di Giandomenico et al. ¹⁵
HEXS	5	1.82		2.46		Skanthakumar et al. ¹³
QM(B3LYP)	5	1.81		2.61		Hay et al. ²⁵
QM(MP2)	5	1.81		2.52		Tsushima et al. ²⁴
QM (B3LYP)	5	1.79		2.55		Pomogaev et al. ⁵⁸
QM (B3LYP)	5	1.79		2.59		Danilo et al. ²⁸
QM (B3LYP)	5	1.78		2.59		Pérez-Conesa et al. ³⁸
MD (300 K)	5	1.80		2.54		Pomogaev et al. ⁵⁸

^aAll experimental EXAFS are obtained at highly acidic pH, with non-coordinating counterions.

The combination of XAS spectroscopy and MD simulations has been revealed as an useful strategy^{30–33} to refine the structural properties of solutions when the standard fitting of the experimental spectra are clouded by different factors as complexity of the system, low concentrations, spectroscopical phenomena as multiexcitations, low signal/noise ratio, and others.³⁴ The good reproduction of an experimental spectrum by means of the use of the structural information derived from a statistical simulation has a double consequence.²³ On the one hand, it allows access to a direct EXAFS structure assignment provided by the atomistic picture of the statistical trajectory. On the other hand, the agreement shows the ability of the interaction potentials employed in the statistical simulation when using classical force fields or the quantum-mechanical level in AIMD simulations to describe properly the system.

Within the actinyl series, PuO₂⁺ has been scarcely studied due to its trend to disproportionate to lower, e.g., Pu⁴⁺, and higher, e.g., PuO₂²⁺, oxidation states. EXAFS studies have dealt with PuO₂⁺ acidic aqueous solutions.^{14,15,20} The main distances, Pu–O_{yl} and Pu–O_l, and the hydration number are collected in Table 1. The EXAFS fitting supplies a reduced range for the main distances, Pu–O_{yl} and Pu–O_l, but the coordination numbers proposed vary from 3.3 to 5.3. Bearing in mind the typical uncertainty in the coordination number

determination from EXAFS fitting due to multiparameter correlation, additional information must be included to elucidate this issue. Some QM calculations had concluded that coordination number is 5 with distances quite different from those obtained by EXAFS, as collected in Table 1.³⁵ Dalodière et al.,²⁰ in a recent study on the PuO₂⁺ aqua ion, showed an interesting synthesis method of this species based on sonochemistry which allowed them to reach millimolar PuO₂⁺ solutions free of other Pu oxidation states. They recorded the EXAFS spectrum of this species and compared it with simulated spectra computed from the QM [PuO₂(H₂O)₅]⁺(H₂O)₁₀ and [PuO₂(H₂O)₄]⁺(H₂O)₈ clusters, obtained by B3LYP optimizations and Debye–Waller factors computed from the QM frequencies of these clusters. They concluded that the best theoretical–experimental agreement corresponds to the PuO₂⁺ tetrahydrate.

In previous works,^{36–38} we have conducted classical MD simulations of actinyls, AnO₂⁺²⁺, in water using interaction potentials based on first-principles QM calculations. EXAFS and XANES spectra have been simulated using the structural information and the theoretical scattering phases and amplitude functions computed by the ab initio FEF code (v.9.6).³⁹ Whereas the theoretical–experimental agreement was quite satisfactory for UO₂²⁺, NpO₂²⁺, and PuO₂²⁺ using

force fields derived from B3LYP potential energy surfaces, the NpO_2^+ case was not satisfactory.³⁸ This fact compelled us to develop for NpO_2^+ a new force field based on QM wave functions with explicit inclusion of the dynamic and non-dynamic electron correlation, as NEVPT2 method does.^{40,41} The simulated EXAFS spectrum gave a fair comparison with the experimental spectra. As far we know, there is not a simulated spectra based on statistical computations for PuO_2^+ , with the coordination number and geometrical parameter remaining controversial.

The aim of this work is to confirm the importance of the use of multideterminantal wave functions as reference QM computations to provide accurate enough force fields when dealing with a higher multiplet open-shell system, as it is that of the PuO_2^+ cation. Likewise, we envisage to develop and test a simpler formulation of the actinyl potential model. For these reasons, we have built a new $\text{NpO}_2^+-\text{H}_2\text{O}$ interaction potential to double check the validity of this new formulation. A revisited analysis of former experimental EXAFS spectra of PuO_2^+ and NpO_2^+ aqueous solutions¹⁵ has also been carried out on the light of the theoretical results.

METHODS

Quantum Chemical Calculations. A main motivation of this study is to get insight into the impact that static and dynamic electron correlation may have on the structure and the dynamical and structural disorder of the close environment of the actinyls. Multireference NEVPT2^{40–42} calculations, which incorporate both types of electron correlation, were conducted using the ORCA⁴³ program. The chosen active space was the set of atomic-like *f*-orbitals in addition to the molecular orbitals resulting from combining actinide *f* orbitals and O_{yl} *p* orbitals. The active space involves 10 molecular orbitals, $2\pi_{\text{w}}$, $3\sigma_{\text{w}}$, $1\phi_{\text{w}}$, $1\delta_{\text{w}}$, $4\sigma_{\text{u}}^*$, and $3\pi_{\text{u}}^*$, as shown by Denning in Figure 1 of his study.⁴⁴ The main atomic orbital composition of these molecular orbitals is given in Table S1. A similar selection was adopted by Gendron et al.⁴⁵ for neptunyl(VI) complexes. This resulted in CASSCF(8,10) configurations for NpO_2^+ and CASSCF(9,10) configurations for PuO_2^+ . A more complete active space would include non bonding, bonding and antibonding molecular orbitals resulting of the inclusion of 6*d* actinide orbitals and their combination with O_{yl} 2*s* and 2*p* orbitals. However, this would lead up to a 16-orbital active space what increased dramatically the number of configurations, e.g., for the PuO_2^+ case the number of configurations for the (9,10) one is $\sim 7 \times 10^3$, whereas for the (15,16) is $\sim 4.9 \times 10^6$. Bearing in mind that we have to deal with the hydrated actinyl aqua ions, both optimizing their geometries and producing a significant numbers of single points to build the interaction potentials, we have adopted the 10-orbital active space also used in precedent studies of complexes of similar sizes.^{28,45} Since the triplet and quartet ground states for NpO_2^+ and PuO_2^+ , respectively, are degenerate, calculations were carried out using a state average over the degenerate states excluding excited states. The perturbational step of the calculation was done using quasi-degenerate perturbation theory. The basis sets used were ma-def2-TZVP for O, def2-SVP for H^{46,47} and SD(60,MWB)//def-TZVP for actinoids.⁴⁸ The calculations were accelerated using the RI and RIJK pseudospectral methods with “autoaux” auxiliary basis sets. Due to the lack of analytical gradients, geometry optimizations were conducted numerically by evenly changing the M– O_{yl} and M– O_1 distances in a 2D grid with a step of ~ 0.005 Å. The structure was assumed to be optimized when the energy of the predicted optimized structure within the grid differs from the QM value obtained for such optimized geometry in less than $10^{-5} E_{\text{h}}$, otherwise a reduced 2D grid, with a smaller step, around this point is computed to estimate the minimum.

Interaction Potentials for AnO_2^+ in Water. To describe the interactions of PuO_2^+ and NpO_2^+ in aqueous solution, we have

developed a procedure based on our statistical implementation of the hydrated ion concept,^{49,50} particularly adapted for the case of monovalent molecular cations.^{36,51} Figure 1 displays a sketch of the interaction potentials involved in the system definition.

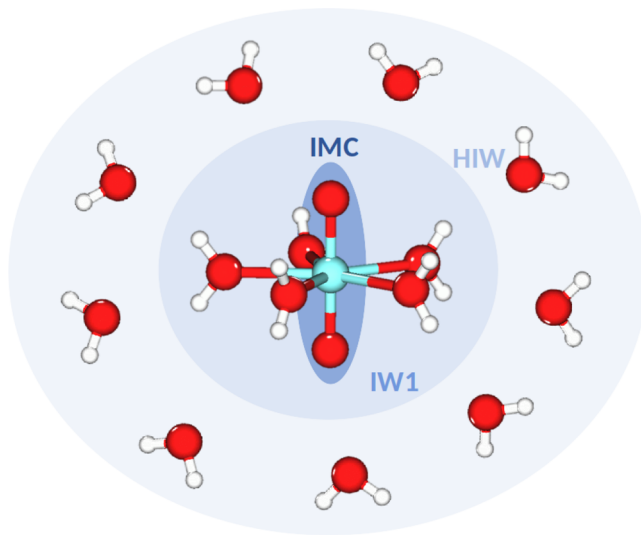


Figure 1. Interaction potentials defined in the system: IMC (intramolecular cation interaction), IW1 (molecular cation–water first-shell interactions), and HIW (hydrated ion–bulk water interactions). The water–water interactions are described by the TIP4P model.⁵²

The basic idea is that the hydrated ion⁵³ is the representative species interacting with the bulk water, ($[\text{AnO}_2(\text{H}_2\text{O})_n]^+-\text{H}_2\text{O}$) by means of a hydrated ion–bulk water potential (HIW). For this aim, the QM interaction energy, $E_{\text{int}}^{\text{QM}}$, is described by two potentials, of which one is the TIP4P potential⁵² that describes the interaction among the first-shell and bulk water molecules and the other collects the interactions between the bulk water molecules and the actinyl cation. The functional form is

$$E_{\text{int}}^{\text{QM}} = E_{\text{HIW}} = \sum_i^{\text{AnO}_2^+ \text{ sites}} \sum_j^{\text{Bulk water sites}} \left(\frac{C_4^{ij}}{r_{ij}^4} + \frac{C_6^{ij}}{r_{ij}^6} + \frac{C_8^{ij}}{r_{ij}^8} + \frac{C_{12}^{ij}}{r_{ij}^{12}} + \frac{q_i q_j}{r_{ij}} \right) + \sum_i^{\text{H}_2\text{O}_1 \text{ sites}} \sum_j^{\text{Bulk water sites}} E_{ij}^{\text{TIP4P}} \quad (1)$$

The interaction of the molecular cation with its first hydration shell (IW1) was parametrized by a series of r^{-n} terms with $n = 4, 6, 8$, and 12 plus the Coulombic term.

$$E_{\text{IW1}} = \sum_i^{\text{AnO}_2 \text{ sites}} \left(\frac{C_4^{i\text{O}}}{r_{i\text{O}}^4} + \frac{C_6^{i\text{O}}}{r_{i\text{O}}^6} + \frac{C_8^{i\text{O}}}{r_{i\text{O}}^8} + \frac{C_{12}^{i\text{O}}}{r_{i\text{O}}^{12}} \right) + \sum_i^{\text{AnO}_2 \text{ sites}} \sum_j^{\text{Water sites}} \frac{q_i q_j}{r_{ij}} \quad (2)$$

At this point it should be noted that the first-shell water molecules are ruled by an interaction potential with the actinyl cation (IW1) different from that of bulk water molecules (HIW). This supplies a refined definition of the interaction within the aqua ion and with the bulk water which allows classical optimized geometries of the aqua ion, as those shown in Table 1, very close to the QM ones, but requiring computational times of seconds instead of tens of hours. The shortcoming associated with this methodological advantage is the fact that no exchange of water molecules between the first-shell and the bulk must occur. Along the MD simulations no water molecule release from the aqua ions to the bulk was observed. Finally, to

describe the intrinsic dynamics of the actinyl cation we have adopted for the intramolecular cation (IMC) potential a new functional form with respect to our previous development.^{36–38,51} We have replaced an interatomic potential based on a power series, as in the E_{HIW} or E_{IW1} functional forms, by an anharmonic potential to describe the An–O_{yl} bonds and a harmonic potential for the bending.

$$E_{\text{IMC}} = \sum_i^{\text{sites}} [k_{\text{An-O}_{yl,i}}(r_i - r_0)^2 + k'_{\text{An-O}_{yl,i}}(r_i - r_0)^3] + k''_{\text{O}_{yl}\text{-An-O}_{yl}}(\theta - \theta_0)^2 \quad (3)$$

Figure 2 displays some representative structures used to build the intermolecular potentials. A total of 64 structures were used for the

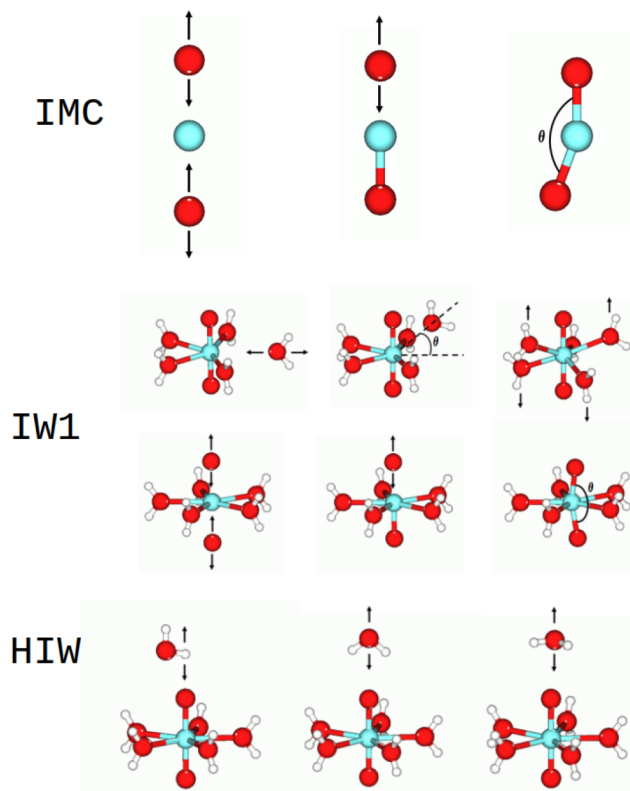


Figure 2. Representative type of structures employed to fit the potentials defined in the system: IMC (intramolecular cation interaction), IW1 (molecular cation–water first-shell interactions), and HIW (hydrated ion–bulk water interactions).

HIW potential, while 220 structures were used for the IW1 and 87 were used for the IMC. For this development, it has been assumed that the aqua ions are pentahydrates. Figures S1 and S2 show the fitting of the set of PuO₂⁺ and NpO₂⁺ potentials. Potential coefficients are given in Tables S2–S5, which include their corresponding standard deviations.

To check the fitted potentials, we have examined the interaction energy of a bulk water molecule approaching the hydrated actinyl from different regions. Figure S3 shows the good correlation between the QM interaction energy and the value predicted by the force field. It must be stressed that these structures were taken from 50 snapshots of an MD simulation where the closest water molecule to the actinyl aqua ion in each angular region was taken.

Given that for the PuO₂⁺ aqueous solution, several authors^{14,15,20} have pointed out that its aqua ion is a tetrahydrate instead of a pentahydrate, a specific force field assuming that the hydrated ion is [PuO₂(H₂O)₄]⁺ was also developed. A fitting procedure similar to that explained for the pentahydrated plutonyl was applied to define

the new IMC potential, and the new PuO₂⁺ polarization on the tetrahydrate was reflected in the Pu and O_{yl} effective charges collected in Table S2. Figure S4 shows the goodness of the fit by comparing the QM interaction energy with the values derived from the IW1 and HIW potentials of the force field.

Molecular Dynamics Simulations. MD simulations were run in a similar way to our previous studies on actinyls.^{36,38,51} A single hydrated actinyl ion, [AnO₂(H₂O)_n]⁺ (An = Np and Pu), and 1490 TIP4P water molecules were placed in a cubic box at the experimental water density. The simulations were run at 300 K in the NVT ensemble using the Noosé–Hoover thermostat with $\tau = 0.5$ ps. Nonbonded interactions were cut at 12 Å, and the Ewald sum was used for the computation of electrostatic interactions. The equations of motion were integrated using a 0.5 fs time step for a total simulation time of 5 ns. All simulations were run using a modified version of DL_POLY Classic⁵⁴ which includes the functional forms of the force field employed. The convergence of MD trajectories has been checked by the analysis of structural, energetic and dynamic properties of the actinyl cations as shown in refs 36, 38, and 51.

The translational self-diffusion coefficient of actinyls, D_{AnO_2} , has been obtained using mean-square displacements (MSD).⁵⁵ This function was computed using multiple time origins up to half of the simulation period for each series. This procedure is particularly appropriate when describing the mobility of only one ion in the system. The 5 ns trajectory was employed to get an average value of D_{AnO_2} , analyzing five series of 1 ns. From it, the average value and an estimation of the error by its standard deviation were conducted. To compute ion hydration enthalpies, ΔH_{hydr} , NPT MD simulations of 1 ns production at 300 K were also conducted. These simulations used the Nosé–Hoover thermostat and barostat with $\tau = 0.5$ ps in both cases. The standard deviation of the average configurational enthalpies was computed by the blocking average method proposed by Flyvbjerg and Petersen⁵⁶ for the error estimation on correlated data.

Simulated XAS Spectra. A total of 500 evenly spaced configurations of [AnO₂(H₂O)_n]⁺ were extracted from 1 ns MD trajectories, i.e., the time interval between two consecutive snapshots is 2 ps, which guarantees noncorrelated statistical information. It has been checked that the use of longer MD trajectories leads to the same simulated spectrum. The configurations included water molecules up to the first solvation shell since we have found the second shell to have no influence on the spectra. Average L_{III}-edge spectra were obtained from the individual spectra using the FEFX code (version 9.6)³⁹ including multiple scattering up to four-legged paths. Details of the spectrum simulation method can be found elsewhere.^{23,31,38,51} An example of the FEFX input files can be found in Figure S5. S_0^2 and ΔE_0 values have been chosen in the simulated NpO₂⁺ and PuO₂⁺ spectrum in order to match the first resonance of the corresponding experimental spectrum.

Experimental EXAFS Spectra. Experimental EXAFS spectra of NpO₂⁺ and PuO₂⁺ aqueous solutions have been recorded as described in ref 15. Revisited analysis of the previous published spectra was conducted with the ATHENA and ARTEMIS codes of Demeter 0.9.25 package⁵⁷ in fluorescence mode for Np and in transmission mode for Pu.

RESULTS AND DISCUSSION

Table 1 collects the An–O_{yl} and An–O_l distances for the two hydrated actinyl cations, [AnO₂(H₂O)_n]⁺ ($n = 4$ and 5), obtained at the QM level by the NEVPT2 method. Likewise, we have included the optimized geometry obtained by using the classical force fields developed (see “POTn (NEVPT2)” rows in the table). It must be underlined that the structural agreement between the QM and force field results is within the hundredth of angstrom. When average distances in solution (see “MD_POTn (300 K)” rows in the table) are considered, it is seen that the An–O_{yl} distance increases slightly ~ 0.017 Å due to solvent effects. For PuO₂⁺, the value of POT5- (NEVPT2) is 1.805 Å, and that for MD_POT5(300 K) is

1.822 Å. For NpO_2^+ , the corresponding values are 1.825 and 1.842 Å. When analyzing the solvent effects for the $\text{An}-\text{O}_1$ distance the change is very small, on the order of 0.001 Å. Thus, Table 1 shows for the PuO_2^+ case that POT5(NEVPT2) gives 2.505 Å, and MD_POT5 (300 K) gives 2.507 Å. For the NpO_2^+ case, the corresponding values are 2.529 and 2.528 Å. As expected, for the hydrate in gas phase, the $\text{Np}-\text{O}_{\text{yl}}$ distance is larger than that of the $\text{Pu}-\text{O}_{\text{yl}}$ and the same trend is observed for the $\text{An}-\text{O}_1$ bond. In water, the hydration effects do not change the gas-phase distance order. For the sake of comparison the scarce experimental data are also collected in Table 1. Our theoretical simulations agree fairly well with available experiments. In the plutonyl case, the experimental EXAFS data presented in this work are also in the narrow range of the previous data. As a matter of fact, no optimization geometry at the highly correlated NEVPT2 level of calculation had been previously reported for plutonyl, and as already observed for the neptunyl case in our previous work on actinyls,³⁸ the most sensitive parameter to the electron correlation is the oxo bond. This effect involves a lengthening of the $\text{Pu}-\text{O}_{\text{yl}}$ bond by 0.05 Å (1.81 Å this work and 1.76 Å with B3LYP),³⁸ and a similar change is observed in this work for neptunyl (1.83 Å) and B3LYP (1.78–1.81 Å).^{25,38,58} This lengthening causes an $\text{An}-\text{O}_1$ distance shortening of some hundredths of an angstrom. For the PuO_2^+ case, the value obtained is 2.51 Å (QM(NEVPT2) for CN = 5 row in Table 1) in this work, whereas the B3LYP values are 2.53 and 2.61 Å.^{58,25} For NpO_2^+ , this work finds 2.52 Å (QM(NEVPT2) for CN = 5 row in Table 1), and previous B3LYP values are in the range of 2.55–2.61 Å.^{25,38,58} In the case of NpO_2^+ , we can compare the performance of the new formulation of the IMC potential, based on harmonic and anharmonic functions, to describe the flexibility of the actinyl entity, with respect to the previous forms, based on a set of r^{-n} powers. The optimized geometry for $[\text{NpO}_2(\text{H}_2\text{O})_5]^+$ using the new potential, POT5(NEVPT2), predicts distance changes smaller than 0.01 Å with respect to the previous values (see values in parentheses in the POT5(NEVPOT2) row).

Due to the sensitivity of the main geometrical parameters to the different QM methods, we have explored for the two actinyl aqua ions the $\text{An}-\text{O}_y$ and $\text{An}-\text{O}_1$ distance change when going from HF to NEVPT2($n,10$) computations. Table 2

Table 2. Optimized Distances (Å) of $[\text{NpO}_2(\text{H}_2\text{O})_5]^+$, $[\text{PuO}_2(\text{H}_2\text{O})_5]^+$, and $[\text{UO}_2(\text{H}_2\text{O})_5]^{2+}$ Obtained via Different QM Methods

method	$[\text{PuO}_2(\text{H}_2\text{O})_5]^+$		$[\text{NpO}_2(\text{H}_2\text{O})_5]^+$		$[\text{UO}_2(\text{H}_2\text{O})_5]^{2+}$	
	$\text{Pu}-\text{O}_{\text{yl}}$	$\text{Pu}-\text{O}_1$	$\text{Np}-\text{O}_{\text{yl}}$	$\text{Np}-\text{O}_1$	$\text{U}-\text{O}_{\text{yl}}$	$\text{U}-\text{O}_1$
HF	1.77	2.53	1.78	2.54	1.74	2.40
CASSCF($n,10$)	1.74	2.63	1.76	2.64		
NEVPT2($n,10$)	1.81	2.51	1.83	2.52		
MP2	1.78	2.42	1.80	2.48	1.78	2.45
B3LYP	1.78	2.55	1.79	2.55		

collects these two optimized distances obtained from different methods. When passing from the HF to CASSCF($n,10$) wave functions, the inclusion of static electron correlation provides multideterminantal wave functions that are eigenfunctions of the total electron spin operators, a quartet for the plutonyl(V) aqua ion and a triplet for the neptunyl(V) aqua ion. This effect shortens by 0.02–0.03 Å the $\text{An}-\text{O}_{\text{yl}}$ and lengthens the $\text{An}-$

O_1 by ~ 0.1 Å. The inclusion of the dynamic correlation into these CASSCF wave functions by means of the NEVPT2 method leads to a significant increase of the oxo-bonds by ~ 0.07 Å what contributes to a strong decreasing of the $\text{An}-\text{O}_1$ by ~ 0.12 Å. For the multideterminantal wave functions of $[\text{PuO}_2(\text{H}_2\text{O})_5]^+$ and $[\text{NpO}_2(\text{H}_2\text{O})_5]^+$ when passing from the CASSCF($n,10$) to the NEVPT2($n,10$), the first-order correction to the wave function is expanded over a set of properly chosen multireference functions which correctly take into consideration the two-electron interactions occurring among the active electrons.⁴² The MP2 method induces a slight increases of the $\text{An}-\text{O}_{\text{yl}}$ bond and a strong decrease of the $\text{An}-\text{O}_1$ with respect to the HF results. This unbalanced effects must be reflecting the fact of perturbing an uncorrelated unrestricted-spin wave function. We have included in the table the case of the uranyl pentahydrate, a closed-shell case, computed at the HF and MP2 level. In this case it is observed how for the one-determinantal wave function, the dynamic electron correlation introduced by MP2 leads to a lengthening of both distances.

The B3LYP method includes an approach of the wave function dynamically correlated via the electron density estimation what leads to modest increases of the $\text{An}-\text{O}_{\text{yl}}$ bond as well as of the $\text{An}-\text{O}_1$. The fact we are dealing with multireferential wave functions makes hard to separate the effects that static and dynamic electron correlation causes on the geometries. Nevertheless, it is generally accepted that the most rigorous way to undertake this type of systems is via a methodology which allows a balanced combination of static and dynamic electron correlation such as the NEVPT2 method provides.^{40,41}

Figure 3 shows the $\text{An}-\text{O}$ and $\text{An}-\text{H}$ RDFs for the NpO_2^+ (red lines) and PuO_2^+ (black lines) cations in aqueous solution derived from the MD simulations. The RDFs of both cations are quite similar, only a slight shifting toward longer distances in the mean values is observed (see Table 1 MD_POTn (300 K) rows) when passing from PuO_2^+ to NpO_2^+ . This is a consequence of the native quantum-mechanical trend observed in the minimized pentahydrates. Thus, the QM gap of $R_{\text{An}-\text{O}_{\text{yl}}}$ between NpO_2^+ and PuO_2^+ hydrates is 0.025 Å, whereas the RDFs shows a gap of 0.02 Å. The trend of the $\text{An}-\text{O}_1$ parameter is similar to that of the $\text{An}-\text{O}_{\text{yl}}$: the $\text{Np}-\text{O}_1$ distance is ~ 0.02 Å longer than that of $\text{Pu}-\text{O}_1$, and the gap in solution is similar because the mean distance changes induced by solvation are only ~ 0.001 Å. The number of water molecules in the second shell is ~ 21 for the two cations, these values are similar to those corresponding to their divalent cations (see Figures 2 and 3 of ref 51).

Figure 4 shows the distribution of water molecules around the different angular regions in one hemisphere that can be defined taking advantage of the system symmetry. The equatorial region ($60-90^\circ$ and $90-120^\circ$) presents two well-defined shells; the $\text{An}-\text{O}$ and $\text{An}-\text{H}$ first peaks correspond to the first hydration shell, already shown in Figure 3, as well as a second hydration shell that integrates to ~ 9.2 molecules centered at 4.8 Å for the oxygen atoms. The comparison for each angular region of the $\text{An}-\text{O}$ and $\text{An}-\text{H}$ peak position sheds light on the relative orientation of water molecules. Thus, in the equatorial region, hydration shells take an ion-dipole orientation, because the $\text{An}-\text{H}$ peak is shifted ~ 0.7 Å from the $\text{An}-\text{O}$ peak. In the intermediate zones ($30-60^\circ$ and $120-150^\circ$), the running integration number is ~ 9 centered far from the actinyl, ~ 4.5 Å, and the $\text{An}-\text{O}$ and $\text{An}-\text{H}$ peaks

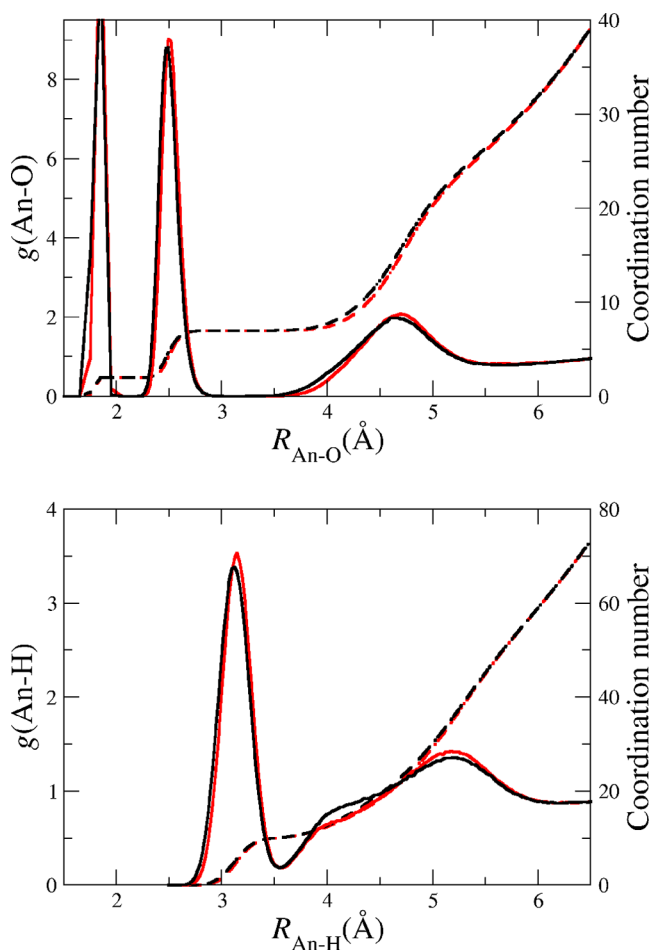


Figure 3. An–O (top) and An–H (bottom) radial distribution functions and their coordination numbers for Np(V) (red) and Pu(V) (black) in aqueous solution as obtained from the MD simulations.

overlap, which means that the water molecules orientation is rather a compromise of their interactions among the molecular cation and the hydration water molecules. In the axial regions, ~ 3.4 molecules are associated with the main peak which is centered at ~ 4.5 Å from the actinide. This rather depopulated axial region shows that hydrogen atoms are closer to the metal cation than to the oxygen atoms due to the presence of O_{yl} atoms. Bearing in mind that the An– O_{yl} distance is ~ 1.8 Å, the mean distance of one water hydrogen atom to the O_{yl} atom is ~ 2.2 Å. This weak hydrogen bond pattern was not found in the previous cases studied of divalent actinyl.⁵¹ The last two regions can be envisaged as hydration structures that build the condensed medium around the aqua ion as well as they solvate slightly the actinyl cation.

Table 3 collects a set of energetic and dynamical properties of the monovalent aqueous solutions. The hydration enthalpies agree well with the estimated experimental values given by Gibson et al.⁵⁹ It must be indicated that the sensitivity of PuO_2^+ electron wave function to its close environment have caused a large uncertainty in the hydration energy among different authors²⁹ as indicated by Ryzhkov et al.³⁵ in their recent study on Pu complexes in water. Taking into account the uncertainties, one can conclude that the hydration enthalpy of both cations is almost the same. Regarding the aqua ion dynamics, their size-corrected diffusion coefficient values for neptunyl and plutonyl are also quite similar. The calculated ion

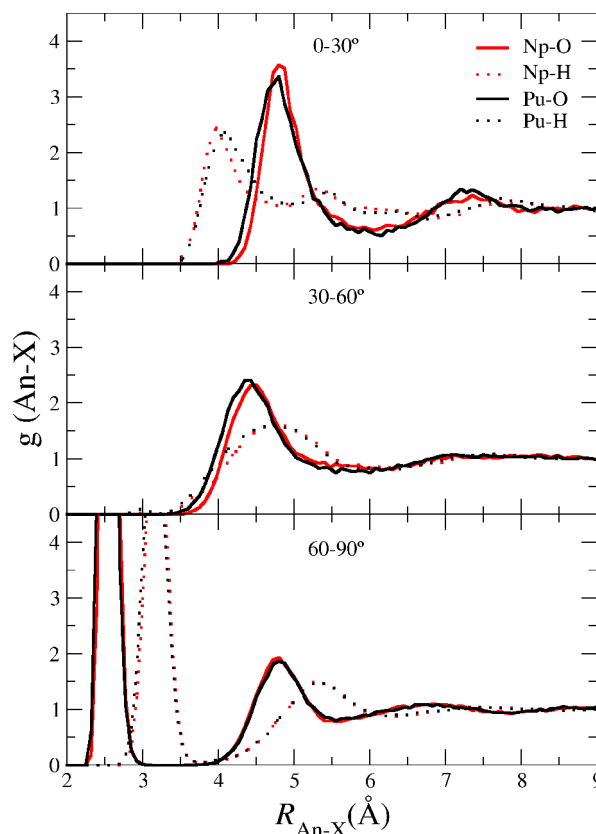


Figure 4. An–O and An–H angle-solved RDFs Np(V) (red) and Pu(V) (black) in aqueous solution as obtained from the MD simulations.

Table 3. Energetic and Dynamical Properties Calculated from the MD Simulations

property	NpO_2^+	PuO_2^+
ΔH_{hyd} (kcal mol ⁻¹)	-166 ± 3	-165 ± 3
ΔH_{hyd}^{exp59} (kcal mol ⁻¹)	-180 ± 20	-178 ± 20
D_{An} (10^{-5} cm ² s ⁻¹)	1.1 ± 0.2	1.1 ± 0.2
D_{An}^{corr} (10^{-5} cm ² s ⁻¹)	1.4 ± 0.2	1.4 ± 0.2
D_{An}/D_w	0.44 ± 0.04	0.43 ± 0.04

mobility is affected by the water mobility, which depends on the water model employed, in our case TIP4P. This model overestimates the water diffusion coefficient, 3.3×10^{-5} cm² s⁻¹,⁶⁰ as the experimental value is 2.3×10^{-5} cm² s⁻¹. For this reason, a better test is needed to compare the values normalized by the water self-diffusion coefficient. The D_{An}/D_w values are 0.44 and 0.43 for NpO_2^+ and PuO_2^+ , respectively. Tiwari et al.⁶¹ have computed the diffusion coefficient for the monovalent actinyls using the SPC/E water model, their normalized values of the size-corrected D_{An}/D_w are 0.46 and 0.45 for NpO_2^+ and PuO_2^+ , respectively. Their corresponding values for the divalent actinyls, NpO_2^{2+} and PuO_2^{2+} , computed in our previous work³⁸ with the same methodology but using a B3LYP-based force field are 0.38, that represents a low limit of diffusion for PuO_2^{2+} and NpO_2^{2+} as they are singly charged. Simonin et al.⁶² have determined experimentally for UO_2^{2+} at infinite dilute aqueous solution a normalized value of 0.30. Our theoretical normalized value for the divalent uranyl, which was also computed in our previous work³⁸ was 0.37.

Another illustrative test of the actinyl dynamics in aqueous solutions is the analysis of the most representative vibrational normal modes. Table 4 shows the symmetric ($1A_1$) and

Table 4. Experimental and MD Normal Mode Frequencies (cm^{-1})

frequencies	method	E_1	$2A_1$	$1A_1$	A_2
[NpO ₂ (H ₂ O) ₅] ⁺	MD (gas phase)	393	251	819	870
	MD (solution)	227	305	798	853
	exp ^{63,64}			767	824
[PuO ₂ (H ₂ O) ₅] ⁺	MD (gas phase)	441	250	780	828
	MD (solution)	276	296	764	811
	exp ⁶⁵			748	

asymmetric (A_2) An–O_{yl} stretching normal modes, the O_{yl}–An–O_{yl} bending (E_1) and the water breathing stretching ($2A_1$). To account for the solvent effects, the gas-phase frequencies of the two pentahydrates have been included in the table. Interestingly, one can observe that for the two actinyl stretching modes the solvation induces redshifts of their frequencies of about 15–20 cm^{-1} . This is a consequence of the interactions with second-shell water molecules in the intermediate and axial regions. On the contrary, solvent effects induce a blueshift of $\sim 50 \text{ cm}^{-1}$ in the water-breathing mode. This is due to the strong aqua ion–water interactions in the equatorial region, where second-shell water molecules causes a compactness of the first-shell water molecules, then increasing the corresponding frequency of the water breathing vibrational mode. Only three experimental frequencies have been reported in the literature;^{63–65} the error of our estimation is smaller than 4% and the sequence predicted by our potentials is the same than the experimental one.

Figures 5 and 6 display the comparison of the experimental EXAFS spectrum reported in the literature from several authors for NpO₂⁺ and PuO₂⁺ in dilute aqueous solutions, together with the revisited spectra previously reported by Di Giandomenico et al.¹⁵ In the NpO₂⁺ case, we can see the reasonable agreement of our simulated spectrum with the three experimental ones.^{9,12,15} Because the experimental difficulties for the X-ray absorption spectrum recording, the difference among the experimental spectra is similar to that observed for the experimental–theoretical comparison. In the bottom of Figure 5 we have included the simulated EXAFS spectrum obtained using our previous NEVPT2-based intermolecular potential.³⁸ This spectrum almost matches the spectrum obtained in this work which employs a simplified version of the intramolecular actinyl potential (IMC).

Regarding the PuO₂⁺ EXAFS spectra, Figure 6 also shows that the differences among them are similar to the relative discrepancy of our simulated spectrum with the three experimental spectra. From the set of EXAFS measurements carried out by one of us on the actinyls in a previous work,¹⁵ the revisited PuO₂⁺ spectrum recorded in transmission mode has been analyzed and included in Figure 6. The spectrum is similar to the spectrum published in that article, although signal/noise is higher as well as global intensity. (cf., “revisited spectrum” in Figure 6 with Pu(V)/HClO₄ in Figure 4 of ref 15). The complicated shape of the EXAFS spectrum is reproduced well by the simulated one in the five oscillations experimentally recorded.

The striking question is the fact that the S_0^2 values needed to match the main oscillations (maximum at $k = 5 \text{ \AA}^{-1}$) are small,

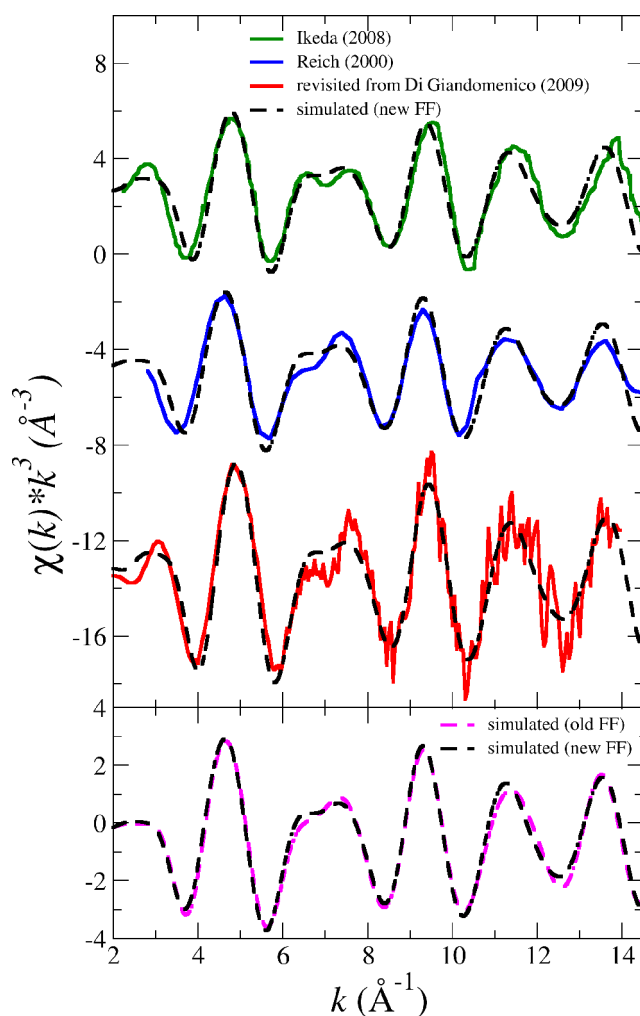
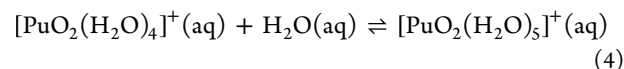


Figure 5. Top: Simulated (dashed black line) vs experimental (solid line green (ref 12), blue (ref 9), red (reanalyzed from ref 15)) Np L_{III}-edge k^3 -weighted EXAFS spectra for NpO₂⁺ in water. Bottom: Comparison between the two simulated EXAFS spectra computed by means of the new NEVPT2 force field developed in this work (black) and the force field developed in a previous work (magenta).³⁸

0.7 for the transmission mode spectrum,¹⁵ 0.6 for that of Dalodière et al.,²⁰ and 0.45 for that of Panak et al. one.¹⁴ In the case of the NpO₂⁺, the values needed are in the range of 0.7–0.9. This fact might be related to the reduction of the coordination number from 5 water molecules in NpO₂⁺ aqueous solution to 4 in the PuO₂⁺ case.

To find out on this issue we have undertaken three additional analysis: (i) quantum-mechanical computation of the relative stability of the two hydrates in water at the same level of calculation employed to develop the force field, (ii) experimental fitting of the previously recorded plutonyl EXAFS spectrum assuming the constraint of a hydration number 4 or 5, and (iii) development a force field for PuO₂⁺ in water based on a tetrahydrate cation and the analysis of results derived from the corresponding MD simulation at 300 K.

A direct procedure to estimate quantum-mechanically the relative stability of [PuO₂(H₂O)₄]⁺ and [PuO₂(H₂O)₅]⁺ in water is the computation of the equilibrium



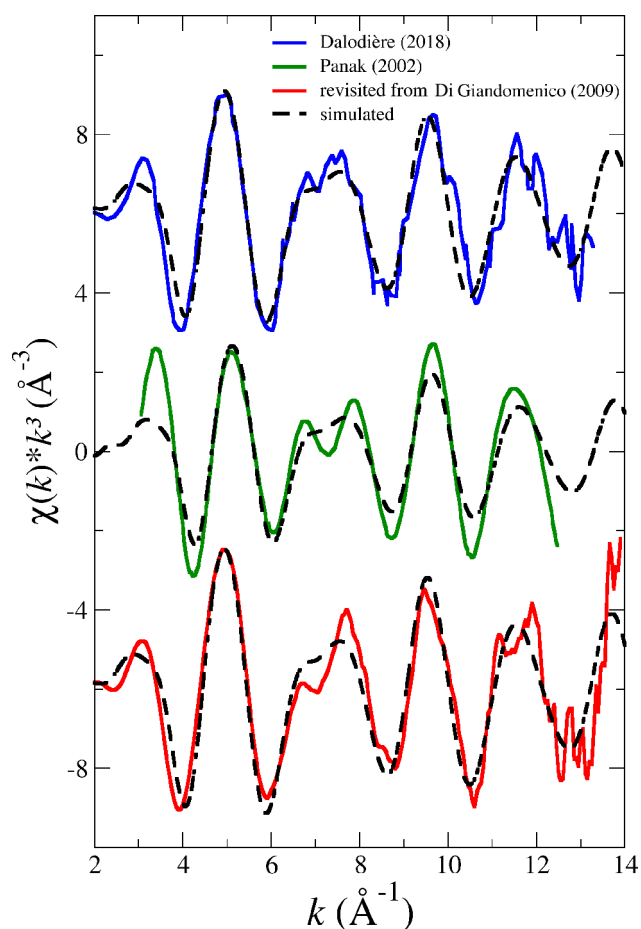
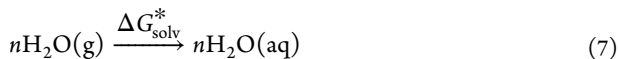
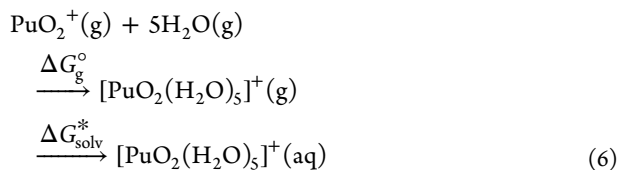
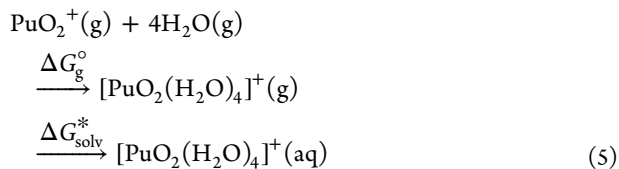


Figure 6. Simulated (dashed black line) vs experimental (solid line blue (ref 20), green (ref 14) and red (reanalyzed from ref 15)) Pu L_{III} -edge k^3 -weighted EXAFS spectra for PuO_2^+ in water.

This equation can be envisaged as the difference between the PuO_2^+ hydration free energy corresponding to the formation of the tetrahydrate and pentahydrate aqua ions in water



The hydration free energy of PuO_2^+ is then computed by the addition of the gas-phase hydrate formation, $\Delta G_{\text{g}}^{\circ}$, its solvation in water, ΔG_{solv}^* , computed by means of the continuum polarizable model,⁶⁶ CPCM,⁶⁷ as implemented in the ORCA program,⁴³ the vaporization free energy of n water and the standard state correction associated with the gas phase-solution transfer, as given by Goddard et al.⁶⁸ The values of the

hydration energy are -124 and -128 kcal/mol for the tetra- and pentahydrate, respectively. Table S6 collects the different contributions to these estimations. From these data, the free energy of eq 4 is -4 kcal/mol, which indicates the preference for the pentahydrate of PuO_2^+ in water from a quantum-mechanical semicontinuum model of solvation.⁶⁹

Figure 7 shows the revisited experimental L_{III} -edge k^3 -weighted EXAFS spectra of NpO_2^+ and PuO_2^+ ¹⁵ and their fits

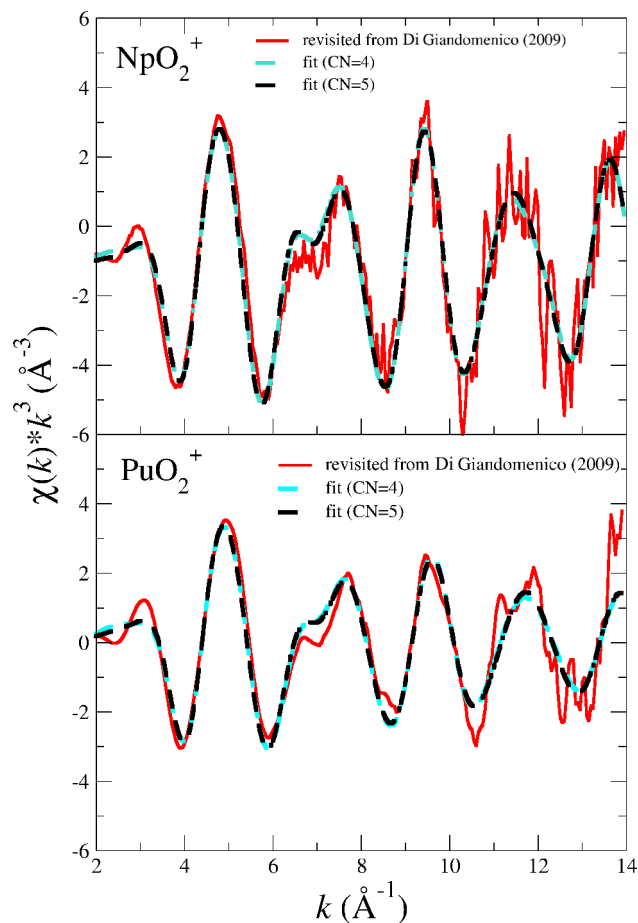


Figure 7. Np (top) and Pu (bottom) L_{III} -edge k^3 -weighted EXAFS spectra for NpO_2^+ and PuO_2^+ in water: experimental (red solid line)¹⁵ and fits assuming a hydration number of four (cyan dashed line) or five (black dashed line).

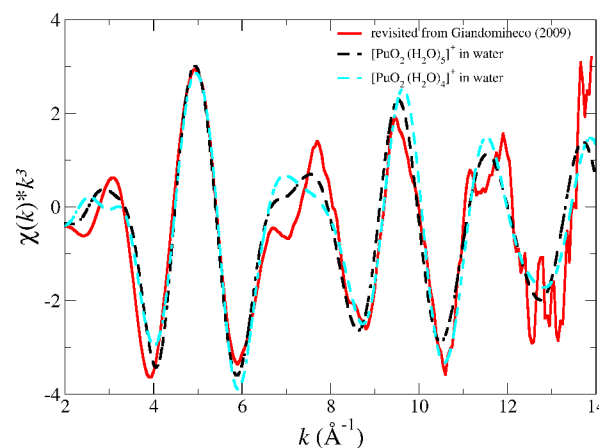
obtained when the first hydration shell is constrained to 4 (cyan dashed line) or 5 (black dashed line). It is observed that the two fits are very similar, and that conclusion is verified by examining Table 5, which collects the main parameters of the fits. This leads to the fact that the assumption of a given coordination number does not change the values of the fitted parameters, since the quality of the fits are almost the same. As already indicated, the sensitivity of the EXAFS for these spectra with such a low signal/noise ratio, due to the high experimental complexity of the measurements, blurs the subtle discrimination of one unit coordination number. Regarding the main An–O distances, one can compare the sequence of distances derived from our MD simulations (MD_POT5 (300 K) rows in Table 1) with the EXAFS fit of Table 5. The trend with the change of actinoid is the same, i.e., $R(\text{NpO}_{\text{yl}}) > R(\text{PuO}_{\text{yl}})$ and $R(\text{NpO}_1) > R(\text{PuO}_1)$. Even more, the distance changes when going from Np to Pu given by MD simulations

Table 5. EXAFS Best-Fit Parameters of NpO_2^+ and PuO_2^+ in HClO_4

fit parameters	NpO_2^+ (CN = 4)	NpO_2^+ (CN = 5)	PuO_2^+ (CN = 4)	PuO_2^+ (CN = 5)
$R(\text{An}-\text{O}_{\text{yl}})$ (Å)	1.83(1)	1.83(1)	1.80(1)	1.80(1)
$\sigma^2(\text{An}-\text{O}_{\text{yl}})$ (Å ²)	0.0003	0.0000	0.0019	0.0015
$R(\text{An}-\text{O}_1)$ (Å)	2.51(1)	2.51(1)	2.47(1)	2.47(1)
$\sigma^2(\text{An}-\text{O}_1)$ (Å ²)	0.0034	0.0044	0.0061	0.0074
S_0^2	0.9	0.8	0.8	0.7
E_0 (eV)	6.0	5.6	6.4	6.1
R_{factor} (%)	2.5	2.6	4.9	6.5

and the EXAFS fittings are close: ΔR_{AnOyl} is -0.02 Å (MD) and -0.03 Å (EXAFS fit); ΔR_{AnO1} is -0.02 Å (MD) and -0.04 Å (EXAFS fit).

The final analysis deals with the use of a force field developed on the basis of the intramolecular and intermolecular interactions of $[\text{PuO}_2(\text{H}_2\text{O})_4]^+$. When running a free MD simulation at 300 K, the plutonyl cation hydration always evolves to a pentahydrate. Pomogaev et al.⁵⁸ in their MD simulations of a set of monovalent actinyl cations showed how the initial tetrahydrate cation, defined as starting hydrated ion, became a pentahydrate when the system evolved. To get a deeper insight into this issue, we envisage a strategy to get a set of snapshots derived from a simulation of a PuO_2^+ aqueous solution, where the cation first-shell was formed by only four water molecules. Toward this aim, we added to our HIW force field for the plutonyl tetrahydrate an additional repulsive Pu–O term, (C/r^{-8}) , that prevented the presence of bulk water molecules inside the first shell. This penalty function vanishes beyond the first shell such as the first-shell–second-shell interactions are those provided by the original force field built from the tetrahydrate. Table 1 collects the main geometrical parameters of the optimized clusters, POT4(NEVPT2) for CN = 4, that compare fairly well with the corresponding QM optimizations of the same hydrates ($R(\text{PuO}_{\text{yl}})$ is 1.800 Å (QM) and 1.795 (POT4) Å; $R(\text{PuO}_1)$ is 2.448 Å (QM) and 2.450 Å (POT4)). The Pu–O and Pu–H RDFs for the MD simulation using POT4(NEVPT2) are plotted in Figure S6, as well as the RDFs derived of the POT5(NEVPT2). The mean values derived from these POT4(NEVPT2) RDFs are also collected in Table 1 and show the same slight changes due to bulk solvent effects already observed for the POT5(NEVPT2) RDFs. Figure 8 compares the simulated EXAFS spectrum of PuO_2^+ in water obtained by the force field developed under the assumption of a pentahydrate, which was already compared with the experimental spectra in Figure 6 and the spectrum obtained with the force field built imposing a tetrahydration. For the sake of comparison, the experimental PuO_2^+ EXAFS spectrum revisited from Di Giandomenico et al.¹⁵ has also been included in Figure 8. Two important facts can be drawn from this figure. The first one is that the tetrahydrate-derived EXAFS does not reproduce the spectrum shape in the peculiar 6–8 Å⁻¹ region. The second one is that the intensity of both spectra is similar, although the coordination number, 5 versus 4, of their first hydration shell could lead to expect a higher intensity for the first spectrum. Certainly, the similarity between both spectra shows the great difficulty to discriminate

**Figure 8.** Simulated Pu L_{III} -edge k^3 -weighted EXAFS spectra for PuO_2^+ in water using the restricted 4 first-shell water molecules force field, POT4(NEVPT2) (cyan), or the pentahydrate force field, (POT5(NEVPT2) (black) vs. the experimental one.¹⁵

a hydration number when experimental signal/noise ratio is low.

The relationship between the change of shape of the PuO_2^+ EXAFS spectrum in the 6–8 Å⁻¹ region and the Pu– O_{yl} and Pu– O_1 distances deserves a final comment. Hydration effects on the aqua ions described by means of the MD simulations, induce changes on the distances which are in the order of 0.01–0.02 Å. The corresponding changes when going from $[\text{PuO}_2(\text{H}_2\text{O})_4]^+$ to $[\text{PuO}_2(\text{H}_2\text{O})_5]^+$ are much more important, in particular, for the An– O_1 distance that increases by ~ 0.05 Å. This is already observed in the QM(NEVPT2) and in the intermolecular potentials developed POT5/4(NEVPT2) optimized structures. Since solvent effects are small, the gap of the Pu– O_1 distance between the tetra- and the pentahydrate holds up in the in-solution simulations MD-POT4/5 (300 K) giving rise to the different shape of the EXAFS spectrum in the 6–8 Å⁻¹ region. This subtle change is responsible for the good agreement found and supports the prevalence of the PuO_2^+ pentahydrate in water. Interestingly, it can be seen how the experimental fittings shown in Table 5 give the same An– O_1 distance for both coordination numbers in order to provide a good reproduction of such challenging region.

CONCLUDING REMARKS

The use of highly correlated wave functions to build the force fields of the paramagnetic actinyls, NpO_2^+ and PuO_2^+ , in aqueous solutions has been shown to improve the accuracy of physicochemical properties of the systems. In particular, the sensitivity of EXAFS spectrum shape to the structural features points out that the comparison of experimental and simulated spectra is a valuable tool to validate the microscopical structure provided by the statistical simulations.

The structural differences between these actinyl cations in aqueous solutions are small. The quantum mechanical description of the aqua ions are already small: $R(\text{Np}-\text{O}_{\text{yl}}) = 1.83$ Å versus $R(\text{Pu}-\text{O}_{\text{yl}}) = 1.81$ Å, and $R(\text{Np}-\text{O}_1) = 2.52$ Å and $R(\text{Pu}-\text{O}_1) = 2.51$ Å. Given that these actinyl aqua ions are monovalent, the impact of the rest of the solvent on their geometries is small, changing only slightly the internal parameters of the aqua ions. They are pentahydrates. This conclusion is based on the quantum-mechanical and statistical descriptions of PuO_2^+ , the similarity observed at the same

calculation level for NpO_2^+ , where the hydration number is widely accepted as 5 and the good agreement with the experimental EXAFS spectra. The tetracoordination proposal based on EXAFS fitting could be biased by the general low intensity of the recorded spectrum signal, for instance, when compared to the neptunyl case. To the generally accepted uncertainty of ± 1 units in the coordination number provided by the EXAFS fitting, we must add the intrinsic experimental difficulties joined to the preparation and recording of these hazardous complexes radioactive samples. Modelization of ionic solutions with ad-hoc intramolecular potentials has helped to refine the analysis of intriguing radioactive species in water and validate future uses of these potentials to further simulations of these radioactive species in water. In particular, the revisiting of previously studied lower computational level actinyl divalent cations,^{37,38} such as PuO_2^{2+} , NpO_2^{2+} , and AmO_2^{2+} , as well as actinoid aqua ions,⁷⁰ appear as challenging next steps in the study of the actinides in aqueous solutions.

■ ASSOCIATED CONTENT

SI Supporting Information

The Supporting Information is available free of charge at <https://pubs.acs.org/doi/10.1021/acs.inorgchem.2c00461>.

Description of the intermolecular potential formalism. Tables with parameters force field obtained for $\text{AnO}_2^+ - \text{H}_2\text{O}$ ($M = \text{Np}, \text{Pu}$). Figures showing the representative set of structure types employed in the fitted potentials. Plots showing the correlation between the QM interaction energies and the predicted values by the developed force field. Examples of input FEFF files used for the XAS spectrum simulations. Details of the QM computation of the PuO_2^+ tetrahydrate and pentahydrate equilibrium. Pu–O and Pu–H RDFs of the MD simulation conducted with the POT4(NEVP2) potential (PDF)

■ AUTHOR INFORMATION

Corresponding Author

Enrique Sánchez Marcos – Department of Physical Chemistry, University of Seville, 41012 Seville, Spain; orcid.org/0000-0002-8367-9105; Phone: +34 955421005; Email: sanchez@us.es

Authors

Gema Raposo-Hernández – Department of Physical Chemistry, University of Seville, 41012 Seville, Spain
José M. Martínez – Department of Physical Chemistry, University of Seville, 41012 Seville, Spain; orcid.org/0000-0002-1792-2197
Rafael R. Pappalardo – Department of Physical Chemistry, University of Seville, 41012 Seville, Spain; orcid.org/0000-0003-3751-2395
Christophe Den Auwer – Université Côte d'Azur, CNRS, ICN, 06108 Nice, France; orcid.org/0000-0003-2880-0280

Complete contact information is available at: <https://pubs.acs.org/doi/10.1021/acs.inorgchem.2c00461>

Notes

The authors declare no competing financial interest.

■ ACKNOWLEDGMENTS

This document is the result of the I+D+i research project PGC2018-099366-B-I00 funded by the Ministerio de Ciencia e Innovación, Agencia Estatal de Investigación (DOI: [10.13039/501100011033](https://doi.org/10.13039/501100011033)) and by ERDF a way of making Europe. G.R.-H. is grateful for a grant associated with the research project FEDER US-1264472 funded by the Junta de Andalucía and University of Sevilla.

■ REFERENCES

- (1) Cotton, S. *Lanthanide & Actinide Chemistry*; Wiley: London, 2006.
- (2) Rizkalla, E. M.; Choppin, G. *Handbook on the Physics and Chemistry of Rare Earths*; Elsevier: North-Holland, 1991; Vol. 15, Chapter 103.
- (3) Aaberg, M.; Ferri, D.; Glaser, J.; Grenthe, I. Structure of the hydrated dioxouranium (VI) ion in aqueous solution. An x-ray diffraction and proton NMR study. *Inorg. Chem.* **1983**, *22*, 3986–3989.
- (4) Allen, P. G.; Bucher, J. J.; Shuh, D. K.; Edelstein, N. M.; Reich, T. Investigation of aquo and chloro complexes of UO_2^{2+} , NpO_2^+ , Np^{3+} , and Pu^{3+} by X-ray absorption fine structure spectroscopy. *Inorg. Chem.* **1997**, *36*, 4676–4683.
- (5) Wahlgren, U.; Moll, H.; Grenthe, I.; Schimmelpfennig, B.; Maron, L.; Vallet, V.; Groppen, O. Structure of Uranium(VI) in Strong Alkaline Solutions. A Combined Theoretical and Experimental Investigation. *J. Phys. Chem. A* **1999**, *103*, 8257–8264.
- (6) McKibben, J. M. Chemistry of the Purex Process. *Radiochim. Acta* **1984**, *36*, 3–15.
- (7) Altmaier, M.; Gaona, X.; Fanghänel, T. Recent Advances in Aqueous Actinide Chemistry and Thermodynamics. *Chem. Rev.* **2013**, *113*, 901–943.
- (8) Bardin, N.; Rubini, P.; Madic, C. Hydration of Actinyl(VI), $\text{MO}_2^{2+}(\text{aq})$ ($M = \text{U}, \text{Np}, \text{Pu}$). An NMR Study. *Radiochim. Acta* **1998**, *83*, 189–194. and references therein.
- (9) Reich, T.; Bernhard, G.; Geipel, G.; Funke, H.; Hennig, C.; Rossberg, A.; Matz, W.; Schell, N.; Nitsche, H. The Rossendorf Beam Line ROBL – a dedicated experimental station for XAFS measurements of actinides and other radionuclides. *Radiochim. Acta* **2000**, *88*, 633–637.
- (10) Antonio, M. R.; Soderholm, L.; Williams, C. W.; Blaudeau, J. P.; Bursten, B. E. Neptunium redox speciation. *Radiochim. Acta* **2001**, *89*, 17–26.
- (11) Neuefeind, J.; Soderholm, L.; Skanthakumar, S. Experimental Coordination Environment of Uranyl(VI) in Aqueous Solution. *J. Phys. Chem. A* **2004**, *108*, 2733–2739.
- (12) Ikeda-Ohno, A.; Hennig, C.; Rossberg, A.; Funke, H.; Scheinost, A. C.; Bernhard, G.; Yaita, T. Electrochemical and complexation behavior of neptunium in aqueous perchlorate and nitrate solutions. *Inorg. Chem.* **2008**, *47*, 8294–8305.
- (13) Skanthakumar, S.; Antonio, M.; Soderholm, L. A Comparison of Neptunyl(V) and Neptunyl(VI) Solution Coordination: The Stability of Cation-Cation Interactions. *Inorg. Chem.* **2008**, *47*, 4591–4595.
- (14) Panak, P.; Booth, C. H.; Caulder, D.; Bucher, J.; Shuh, D.; Nitsche, H. X-ray absorption fine structure spectroscopy of plutonium complexes with bacillus sphaericus. *Radiochim. Acta* **2002**, *90*, 315–321.
- (15) Di Giandomenico, M. V.; Le Naour, C.; Simoni, E.; Guillaumont, D.; Moisy, P.; Hennig, C.; Conradson, S. D.; Den Auwer, C. Structure of early actinides(V) in acidic solutions. *Radiochim. Acta* **2009**, *97*, 347–353.
- (16) Odoh, S.; Bylaska, E.; de Jong, W. Coordination and hydrolysis of Plutonium ions in aqueous solution using Car-Parrinello molecular dynamics free energy simulations. *J. Phys. Chem. A* **2013**, *117*, 12256–12267.
- (17) Denecke, M. A. Actinide Speciation Using X-Ray Absorption Fine Structure Spectroscopy. *Coord. Chem. Rev.* **2006**, *250*, 730–754.

- (18) Conradson, S. D. Application of X-ray absorption fine structure spectroscopy to materials and environmental science. *Appl. Spectrosc.* **1998**, *52*, 252A–279A.
- (19) Knope, K. E.; Soderholm, L. Solution and Solid-State Structural Chemistry of Actinide Hydrates and Their Hydrolysis and Condensation Products. *Chem. Rev.* **2013**, *113*, 944–994.
- (20) Dalodière, E.; Virost, M.; Dumas, T.; Guillaumont, D.; Illy, M.; Berthon, C.; Guerin, L.; Rossberg, A.; Venault, L.; Moisy, P.; Nikitenko, S. I. Structural and magnetic susceptibility characterization of Pu(V) aqua ion using sonochemistry as a facile synthesis method. *Inorg. Chem. Front.* **2018**, *5*, 100–111.
- (21) Reich, T.; Geipel, G.; Funke, H.; Hennig, C.; Roßberg, A.; Bernhard, G. XANES and EXAFS measurements of plutonium hydrates. In *Biannual Report 1999/2000, FZR-322; Project-Group ESRF-Beamline (ROBL-CRG)*, 2001; pp 27–32.
- (22) Hennig, C.; Schmeide, K.; Brendler, V.; Moll, H.; Tsushima, S.; Scheinost, A. C. EXAFS Investigation of U(VI), U(IV), and Th(IV) Sulfate Complexes in Aqueous Solution. *Inorg. Chem.* **2007**, *46*, 5882–5892.
- (23) Galbis, E.; Hernández-Cobos, J.; Den Auwer, C.; Le Naour, C.; Guillaumont, D.; Simoni, E.; Pappalardo, R. R.; Sánchez Marcos, E. Solving the Hydration Structure of the Heaviest Actinide Aqua Ion Known: The Californium (III) Case. *Angew. Chem., Int. Ed.* **2010**, *122*, 3899–3903.
- (24) Tsushima, S.; Suzuki, A. Hydration numbers of pentavalent and hexavalent uranyl, neptunyl, and plutonyl. *J. Mol. Struct.(THEOCHEM)* **2000**, *529*, 21–25.
- (25) Hay, P. J.; Martin, R. L.; Schreckenbach, G. Theoretical Studies of the Properties and Solution Chemistry of AnO_2^{2+} and AnO_2^+ Aquo Complexes for An = U, Np, and Pu. *J. Phys. Chem. A* **2000**, *104*, 6259–6270.
- (26) Moskaleva, L.; Krüger, S.; Spörl, A.; Rösch, N. Role of Solvation in the Reduction of the Uranyl Dication by Water: A Density Functional Study. *Inorg. Chem.* **2004**, *43*, 4080–4090.
- (27) Gutowski, K.; Dixon, D. Predicting the Energy of the Water Exchange Reaction and Free Energy of Solvation for the Uranyl Ion in Aqueous Solution. *J. Phys. Chem. A* **2006**, *110*, 8840–8856.
- (28) Danilo, C.; Vallet, V.; Flament, J.-P.; Wahlgren, U. Effects of the first hydration sphere and the bulk solvent on the spectra of the f2 isoelectronic actinide compounds: U^{4+} , NpO_2^+ , and PuO_2^{2+} . *Phys. Chem. Chem. Phys.* **2010**, *12*, 1116–1130.
- (29) Clark, A. E.; Samuels, A.; Wisuri, K.; Landstrom, S.; Saul, T. Sensitivity of Solvation Environment to Oxidation State and Position in the Early Actinide Period. *Inorg. Chem.* **2015**, *54*, 6216–6225.
- (30) Palmer, B. J.; Pfund, D. M.; Fulton, J. L. Direct Modeling of EXAFS Spectra from Molecular Dynamics Simulations. *J. Phys. Chem.* **1996**, *100*, 13393–13398.
- (31) Merkling, P. J.; Muñoz-Páez, A.; Sánchez Marcos, E. Exploring the Capabilities of X-Ray Absorption Spectroscopy for Determining the Structure of Electrolyte Solutions: Computed Spectra for Cr^{3+} or Rh^{3+} in Water Based on Molecular Dynamics. *J. Am. Chem. Soc.* **2002**, *124*, 10911–10920.
- (32) Muñoz-Páez, A.; Sánchez Marcos, E. In *Comprehensive Inorganic Chemistry II: From Elements to Applications*, 2nd ed.; Reedijk, J., Poepelmeier, K., Eds.; Elsevier, 2013; Vol. 9, pp 133–159.
- (33) D'Angelo, P.; Martelli, F.; Spezia, R.; Filipponi, A.; Denecke, M. A. Hydration Properties and Ionic Radii of Actinide (III) Ions in Aqueous Solution. *Inorg. Chem.* **2013**, *52*, 10318–10324.
- (34) Provost, K.; Beret, E. C.; Bouvet Muller, D.; Michalowicz, A.; Sánchez Marcos, E. EXAFS Debye-Waller factors issued from Car-Parrinello molecular dynamics: Application to the fit of oxaliplatin and derivatives. *J. Chem. Phys.* **2013**, *138*, 084303.
- (35) Ryzhkov, M. V.; Enyashin, A. N.; Delley, B. Plutonium complexes in water: new approach to ab initio modeling. *Radiochim. Acta* **2021**, *109*, 327–342.
- (36) Pérez-Conesa, S.; Torrico, F.; Martínez, J. M.; Pappalardo, R. R.; Sánchez Marcos, E. A Hydrated Ion Model of $[\text{UO}_2]^{2+}$ in Water: Structure, Dynamics, and Spectroscopy from Classical Molecular Dynamics. *J. Chem. Phys.* **2016**, *145*, 224502.
- (37) Pérez-Conesa, S.; Martínez, J. M.; Pappalardo, R. R.; Sánchez Marcos, E. Extracting the Americium Hydration from an Americium Cationic Mixture in Solution: A Combined X-ray Absorption Spectroscopy and Molecular Dynamics Study. *Inorg. Chem.* **2018**, *57*, 8089–8097.
- (38) Pérez-Conesa, S.; Martínez, J. M.; Pappalardo, R. R.; Sánchez Marcos, E. Combining EXAFS and computer simulations to refine the structural description of actinyls in water. *Molecules* **2020**, *25*, No. 5250.
- (39) Rehr, J. J.; Kas, J. J.; Vila, F. D.; Prange, M. P.; Jorissen, K. Parameter-free calculations of x-ray spectra with FEFF9. *Phys. Chem. Chem. Phys.* **2010**, *12*, 5503–5513.
- (40) Angeli, C.; Cimiriaglia, R.; Malrieu, J.-P. N-electron valence state perturbation theory: a fast implementation of the strongly contracted variant. *Chem. Phys. Lett.* **2001**, *350*, 297–305.
- (41) Angeli, C.; Cimiriaglia, R.; Malrieu, J.-P. n-electron valence state perturbation theory: A spinless formulation and an efficient implementation of the strongly contracted and of the partially contracted variants. *J. Chem. Phys.* **2002**, *117*, 9138–9153.
- (42) Angeli, C.; Cimiriaglia, R.; Evangelisti, S.; Leininger, T.; Malrieu, J.-P. Introduction of n-electron valence states for multi-reference perturbation theory. *J. Chem. Phys.* **2001**, *114*, 10252–10264.
- (43) Neese, F.; Wennmohs, F.; Becker, U.; Riplinger, C. The ORCA quantum chemistry program package. *J. Chem. Phys.* **2020**, *152*, 224108.
- (44) Denning, R. G. Electronic Structure and Bonding in Actinyl Ions and their Analogs. *J. Phys. Chem. A* **2007**, *111*, 4125–4143.
- (45) Gendron, F.; Páez-Hernández, D.; Notter, F.-P.; Pritchard, B.; Bolvin, H.; Autschbach, J. Magnetic Properties and Electronic Structure of Neptunyl(VI) Complexes: Wavefunctions, Orbitals, and Crystal-Field Models. *Chem. - Eur. J.* **2014**, *20*, 7994–8011.
- (46) Zheng, J.; Xu, X.; Truhlar, D. Minimally augmented Karlsruhe basis sets. *Theor. Chem. Acc.* **2011**, *128*, 295–305.
- (47) Weigend, F.; Ahlrichs, R. Balanced basis sets of split valence, triple zeta valence and quadruple zeta valence quality for H to Rn: Design and assessment of accuracy. *Phys. Chem. Chem. Phys.* **2005**, *7*, 3297–3305.
- (48) Cao, X.; Dolg, M.; Stoll, H. Valence basis sets for relativistic energy-consistent small-core actinide pseudopotentials. *J. Chem. Phys.* **2003**, *118*, 487–496.
- (49) Pappalardo, R. R.; Sánchez Marcos, E. Recovering the concept of the Hydrated Ion for model ionic solutions: A Monte Carlo study of the Zn^{2+} in water. *J. Phys. Chem.* **1993**, *97*, 4500–4504.
- (50) Martínez, J. M.; Pappalardo, R. R.; Sánchez Marcos, E. First-principles Ion-Water interaction potentials for highly charged monoatomic cations. Computer simulations of Al^{3+} , Mg^{2+} and Be^{2+} . *J. Am. Chem. Soc.* **1999**, *121*, 3175–3184.
- (51) Pérez-Conesa, S.; Torrico, F.; Martínez, J. M.; Pappalardo, R. R.; Sánchez Marcos, E. A General Study of Actinyl Hydration by Molecular Dynamics Simulations Using ab initio Force Fields. *J. Chem. Phys.* **2019**, *150*, 104504.
- (52) Jorgensen, W. L.; Chandrasekhar, J.; Madura, J. D.; Impey, R. W.; Klein, M. L. Comparison of Simple Potential Functions for Simulating Liquid Water. *J. Chem. Phys.* **1983**, *79*, 926–935.
- (53) Richens, D. T. *The Chemistry of Aqua Ions*; John Wiley: Chichester, U.K., 1997.
- (54) Todorov, I. T.; Smith, W.; Trachenko, K.; Dove, M. T. DL_POLY_3: New Dimensions in Molecular Dynamics Simulations Via Massive Parallelism. *J. Mater. Chem.* **2006**, *16*, 1911–1918.
- (55) Allen, M.; Tildesley, D. *Computer Simulation of Liquids*; Clarendon Press: New York, 1983; Chapter 6.
- (56) Flyvbjerg, H.; Petersen, H. G. Error Estimates on Averages of Correlated Data. *J. Chem. Phys.* **1989**, *91*, 461–466.
- (57) Ravel, B.; Newville, M. ATHENA, ARTEMIS, HEPHAESTUS: data analysis for X-ray absorption spectroscopy using IFEFFIT. *J. Synchrotron Radiat.* **2005**, *12*, 537–541.

(58) Pomogaev, V.; Tiwari, S. P.; Rai, N.; Goff, G. S.; Runde, W.; Schneider, W. F.; Maginn, E. J. Development and Application of Effective Pairwise Potentials for UO_2^{n+} , NpO_2^{n+} , PuO_2^{n+} , and AmO_2^{n+} ($n = 1, 2$) Ions With Water. *Phys. Chem. Chem. Phys.* **2013**, *15*, 15954–15963.

(59) Gibson, J. K.; Haire, R. G.; Santos, M.; Marçalo, J.; Pires de Matos, A. Oxidation Studies of Dipositive Actinide Ions, An^{2+} ($\text{An} = \text{Th}, \text{U}, \text{Np}, \text{Pu}, \text{Am}$) in the Gas Phase: Synthesis and Characterization of the Isolated Uranyl, Neptunyl, and Plutonyl Ions $\text{UO}_2^{2+}(\text{g})$, $\text{NpO}_2^{2+}(\text{g})$ and $\text{PuO}_2^{2+}(\text{g})$. *J. Phys. Chem. A* **2005**, *109*, 2768–2781.

(60) Watanabe, K.; Klein, M. L. Effective Pair Potentials and the Properties of Water. *Chem. Phys.* **1989**, *131*, 157–167.

(61) Tiwari, S. P.; Rai, N.; Maginn, E. J. Dynamics of Actinyl Ions in Water: A Molecular Dynamics Simulation Study. *Phys. Chem. Chem. Phys.* **2014**, *16*, 8060–8069.

(62) Simonin, J.-P.; Billard, I.; Hendrawan, H.; Bernard, O.; Lützenkirchen, K.; Sémon, L. Study of kinetic electrolyte effects on a fast reaction in solution: The quenching of fluorescence of uranyl ion up to high electrolyte concentration. *Phys. Chem. Chem. Phys.* **2003**, *5*, 520–527.

(63) Basile, L. J.; Sullivan, J. C.; Ferraro, J. R.; LaBonville, P. The Raman scattering of uranyl and transuranium V, VI, and VII ions. *Appl. Spectrosc.* **1974**, *28*, 142–145.

(64) Jones, L. H.; Penneman, R. A. Infrared spectra and structure of uranyl and transuranium (V) and (VI) ions in aqueous perchloric acid solution. *J. Chem. Phys.* **1953**, *21*, 542–544.

(65) Madic, C.; Begun, G. M.; Hobart, D. E.; Hahn, R. L. Raman Spectroscopy of Neptunyl and Plutonyl Ions in Aqueous Solution: Hydrolysis of $\text{Np}(\text{VI})$ and $\text{Pu}(\text{VI})$ and Disproportionation of $\text{Pu}(\text{V})$. *Inorg. Chem.* **1984**, *23*, 1914–1921.

(66) Tomasi, J.; Mennucci, B.; Cammi, R. Quantum mechanical continuum solvation models. *Chem Rev.* **2005**, *105*, 2999–3094.

(67) Barone, V.; Cossi, M. Quantum Calculation of Molecular Energies and Energy Gradients in Solution by a Conductor Solvent Model. *J. Phys. Chem. A* **1998**, *102*, 1995–2001.

(68) Bryantsev, V. S.; Diallo, M. S.; Goddard, W. A., III Calculation of Solvation Free Energies of Charged Solutes Using Mixed Cluster/Continuum Models. *J. Phys. Chem. B* **2008**, *112*, 9709–9719.

(69) Martínez, J.; Pappalardo, R.; Sánchez Marcos, E.; Mennucci, B.; Tomasi, J. Analysis of the Opposite Solvent Effects Caused by Different Solute Cavities on the Metal-Water Distance of Monoatomic Cation Hydrates. *J. Phys. Chem. B* **2002**, *106*, 1118–1123.

(70) Caralampio, D.; Martínez, J. M.; Pappalardo, R. R.; Sánchez Marcos, E. Hydration Structure of the Elusive $\text{Ac}(\text{III})$ Aqua Ion: Interpretation of X-ray Absorption Spectroscopy (XAS) Spectra on the Basis of Molecular Dynamics (MD) Simulations. *Inorg. Chem.* **2019**, *58*, 2777–2783.